Quantification of Regional Left Ventricular Dyssynchrony by Magnetic Resonance Imaging

Massimo Mischi*, *Member, IEEE*, Harrie C. M. van den Bosch, Annemieke H. M. Jansen, Mischa Sieben, Ronald M. Aarts, *Fellow, IEEE*, and Hendrikus H. M. Korsten

***Abstract*—Cardiac resynchronization therapy is an established treatment in patients with symptomatic heart failure and intraventricular conduction delay. Electrical dyssynchrony is typically adopted to represent myocardial activation dyssynchrony, which should be compensated by cardiac resynchronization therapy. One third of the patients, however, does not respond to the therapy. Therefore, imaging modalities aimed at the mechanical dyssynchrony estimation have been recently proposed to improve patient selection criteria. This paper presents a novel fully automated method for regional mechanical left ventricular dyssynchrony quantification in short-axis magnetic resonance imaging. The endocardial movement is described by time-displacement curves with respect to an automatically determined reference point. Different methods are proposed for time-displacement curve analysis aimed at the regional contraction timing estimation. These methods were evaluated in two groups of subjects with (nine patients) and without (six patients) left bundle branch block. The contraction timing standard deviation showed a significant increase for left bundle branch block patients with all the methods. A novel method based on phase spectrum analysis may be however preferred due to a better specificity (99.7%) and sensitivity (99.0%). In conclusion, this method provides a valuable prognostic indicator for heart failure patients with dyssynchronous ventricular contraction and it opens new possibilities for regional timing analysis.**

***Index Terms*—Biomedical measurement, cardiology, magnetic resonance imaging (MRI), medical image processing.**

I. Introduction

IN THE UNITED STATES alone, there are about five million chronic heart failure (CHF) patients, with an incidence of about half million new cases a year [1]. Approximately one third of the CHF population suffers from conduction system disease, i.e., the electrical depolarization signal that induces the muscle contraction is not properly conducted over the myocardium [2]. This is typically characterized by a prolongation of the QRS complex (corresponding to the ventricular depolarization) in the electrocardiographic measurement [3].

If the conduction system functions properly, the myocardium thickens and moves coherently inward during contraction (systole). If a conductive block is present, the electrical activation time of the ventricular segments becomes more differentiated, leading to dyssynchronous mechanical movements [4]. The major effects of a dyssynchronous contraction consist of a reduction of cardiac efficiency and ejection fraction, leading to a progressive left ventricle (LV) dilatation and deterioration of the LV function [5]–[8].

Recently, cardiac resynchronization therapy (CRT) has become an additional established therapy for patients with symptomatic heart failure and prolonged QRS duration. Large multicenter trials have shown that CRT improves symptoms, LV function, and prolongs survival [7], [9], [10]. Nevertheless, not all patients respond to CRT. Symptomatic improvement is achieved in approximately 70% of patients while LV reverse remodeling [11] is appreciated in slightly more than 50% of patients. In order to explain the lack of response, attention has been given to inappropriate patient selection and, in particular, to the predictive value of the QRS duration [12]–[18].

Initially, the electrical dyssynchrony was considered representative for the LV mechanical dyssynchrony. However, the poor predictive value of QRS duration to select CRT responders and several studies on mechanical dyssynchrony suggest that mechanical dyssynchrony is a better predictor for CRT response than electrical dyssynchrony [19]–[21]. In addition, patients with a normal QRS duration can also have mechanical dyssynchrony [17].

Mechanical dyssynchrony can be assessed using imaging modalities based on magnetic resonance imaging (MRI) or ultrasound echo-Doppler. In general, myocardial velocity timing can be evaluated by ultrasound tissue Doppler imaging (TDI) [16], [20], [22] and myocardial strain timing can be evaluated by MRI tagging [23], [24]. However, TDI is limited by the acoustic windows through the ribs and the anisotropic sensitivity of the method (Doppler frequency shifts only occur for longitudinal motion), while MRI tagging requires extensive computation and shows a low sensitivity for reduced wall thickening (hypokinetic ventricle). All these methods, moreover, estimate the contraction timing based on one single moment of the cardiac cycle, e.g., the end systolic time.

Manuscript received January 17, 2007; revised July 3, 2007. *Asterisk indicates corresponding author.*

*M. Mischi is with the Department of Electrical Engineering, Eindhoven University of Technology, P.O. Box 513, Eindhoven 5600 MB, The Netherlands (e-mail: m.mischi@tue.nl).

H. C. M. van den Bosch is with the Department of Radiology, Catharina Hospital, Eindhoven 5623 EJ, The Netherlands.

A. H. M. Jansen is with the Department of Cardiology, Catharina Hospital, Eindhoven 5623 EJ, The Netherlands.

M. Sieben is with the Department of Electrical Engineering, Eindhoven University of Technology, Eindhoven 5600 MB, The Netherlands.

R. M. Aarts is with the Philips Research, Eindhoven 5656 AE, The Netherlands and also with the Department of Electrical Engineering, Eindhoven University of Technology, Eindhoven 5600 MB, The Netherlands.

H. H. M. Korsten is with the Department of Anesthesiology, Catharina Hospital, Eindhoven, The Netherlands and also with the Department of Electrical Engineering, Eindhoven University of Technology, Eindhoven 5600 MB, The Netherlands.

Color versions of one or more of the figures in this paper are available online at http://ieeexplore.ieee.org.

Digital Object Identifier 10.1109/TBME.2008.915724

Due to the limited means to study the mechanical synchronicity of the myocardial movement, other alternative medical imaging methods have been recently proposed in the literature. They make use of endocardial segmentation and tracking to derive novel prognostic parameters for dyssynchrony evaluation [25], [26]. However, these methods are still under development and a gold standard for dyssynchrony quantification, apart from the QRS prolongation, does not exist.

When endocardial wall tracking techniques are employed for synchronicity measurements, a fundamental issue is the reliability of the LV segmentation. Today, robust and accurate segmentation remains complicated to achieve. As a result, in clinical practice, the segmentation procedure is usually performed manually by cardiologists or radiologists.

In this paper, we present a new method for regional dyssynchrony quantification that is fully automatic, limiting the user dependency of the measurement to the image acquisition. The need for a robust segmentation has directed our preference to the use of MRI, since magnetic resonance images show a high contrast along the endocardial contour. Despite its 3-D nature, the ventricular motion can be also studied in a 2-D short-axis or long-axis view [26]–[28]. In particular, a short-axis basal view permits to assess the synchronicity of the basal segments, which is reported to be of prognostic value for CRT evaluation [15], [19]. This allows reducing the diagnostic system complexity from three to two dimensions.

Several options are available from the literature for the detection (segmentation) of the endocardial contour [29], ranging from morphologic segmentation [30] to the use of active appearance models [31]–[33], active contour models [34], and level set methods [35]. The initialization of the segmentation process, however, usually requires the manual input of landmarks or even the manual definition of a "first guess" contour.

In this study, we propose a development of the algorithm presented in [36]. This method, first applied in the context of the indicator dilution analysis for the definition of an optimal region of interest (ROI), showed sufficient accuracy to be extended to other applications. The choice for this method is motivated by its radial structure, especially suitable for the detection of a convex contour, such as the endocardium in a short-axis view (see Fig. 1). Unlike methods using explicit model parametrization for the contour detection, this method is more general, due to the absence of a contour descriptor (model).

The method in [36] detects the endocardium along a beam of rays originating in the ventricular center, referred to as a seed point. The seed point position is manually defined by the user. The reduction of the contour detection to a monodimensional problem decreases the computational complexity of the algorithm. A monodimensional high-pass filter operates on the intensity (gray levels) profile along the rays. A boundary point is defined as the location where the output of this filter surpasses a determined threshold. The threshold is determined on the basis of the image histogram.

Here, we propose two major improvements to the segmentation algorithm in the initialization and the contour-detection phase.

- The initialization is fully automated by addition of a preprocessing stage, where the location of the LV is automatically detected. As a result, the seed point is also automatically determined and the segmentation, in contrast to several published methods, is not based on the manual input of landmarks [29], [32]. The LV is recognized in the adopted short-axis view as the structure with the maximum concentric movement of its contour during one cardiac cycle.
- The critical need for the determination of a threshold is avoided by integrating and optimizing the algorithm reported in [37], which is based on multiscale and fuzzy logic analysis. This leads to an accurate localization of the endocardial boundary in a noisy image without the need for the determination of an appropriate threshold [38], which is a critical issue for several segmentation algorithms.

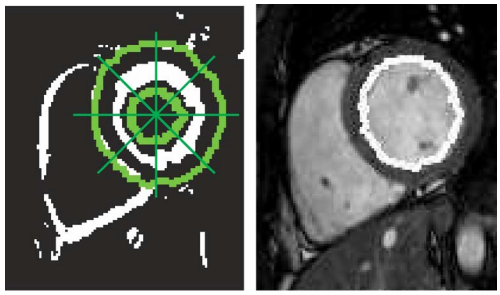

(a) Motion (b) Tracked contour

Fig. 1. Short-axis basal view of the left ventricle. (a) The region of interest in the motion image (b) used for detecting and tracking the endocardium is circumscribed by inner and outer bounds on a beam of rays originating in the ventricular center, i.e., the seed point. The number of displayed rays is limited to eight for illustrative purposes. The papillary muscles are dark structures inside the detected and tracked contour.

The feasibility of the proposed fully automated segmentation method was tested on MRI scans of subjects with and without left bundle branch block (LBBB) in the conduction system. The segmentation accuracy was validated against manual segmentation with satisfactory results.

In this study, segmentation is an essential tool, but it is not the core of the analysis. Once the endocardial contour and seed point are automatically determined, time-displacement curves (TDCs) are derived and used to describe the regional motion of the endocardial segments with respect to the seed point. Rather than limiting the analysis to one moment in the cardiac cycle, e.g., the systole [15], [25], we also propose methods that use the entire cardiac cycle to establish the mutual mechanical time delays between the ventricular basal segments.

A method that was presented in the literature for contraction dyssynchrony assessment based on the analysis of the complete cardiac cycle assumes the TDC to be characterized by a sinusoidal function [26], [28], [39]. Under this assumption, the mutual delay between two TDCs can be derived from their inner product. This approach can be, therefore, adapted to calculate the delays along the entire endocardial contour in the adopted basal view.

In order to avoid the assumption of sinusoidal TDCs, which is not always realistic, here we also propose and test a cross-correlation method for the dyssynchrony assessment based on TDC analysis. The cross-correlation maximum defines the regional contraction timing. This approach enables integration of

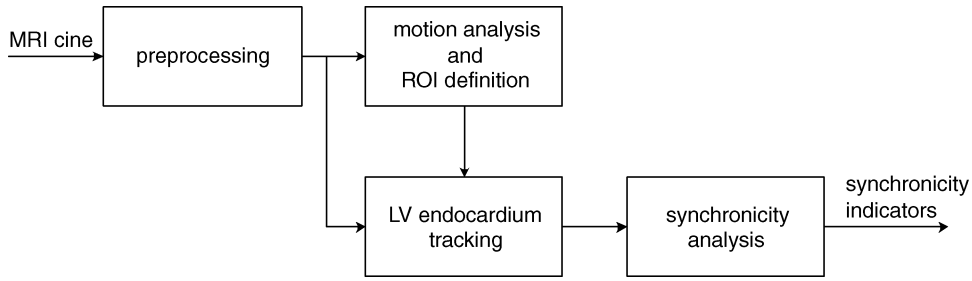

Fig. 2. General scheme of the algorithm for dyssynchrony analysis. After preprocessing the acquired MRI cine, a region of interest based on the analysis of moving strictures is defined and used for the LV endocardium tracking. The resulting spatio–temporal information is then used to assess the intraventricular dyssynchrony.

a dynamic window in the cross-correlation analysis for the extraction of coherent contraction timings. As a result, only active septal movements are processed, while passive paradoxical movements of the septum are excluded [40], [41].

Despite the use of fast MRI pulse sequences, the time resolution of the system for timing measurements is limited. Since the TDCs are delayed versions of approximately the same curve, the time resolution limitation can be solved by determining and processing the phase-difference spectrum of the curves [42].

The developed synchronicity analysis methods were validated on two groups of patients with and without LBBB. The cross-correlation and phase difference methods were tested on the two groups of patients together with the inner product and systolic time method, also applied along the endocardial contour in the adopted basal short-axis view.

II. Methodology

This section reports the steps of the proposed algorithm, which, as shown in Fig. 2, can be defined as follows.

- MRI cine acquisition of a basal short-axis view and preprocessing to improve image quality (Section II-A).
- Automatic definition of an ROI around the endocardium to reduce the image segmentation area and improve the robustness of the following endocardium detection (Section II-B). The ROI definition is based on motion analysis and does not require any user interaction.
- Endocardium detection and tracking based on a radial filter centered in the ROI (Section II-C). The filter is an improvement of that proposed in [36] by integration of multiscale analysis, so that no threshold definition is required.
- Intraventricular synchronicity estimation based on the analysis of the endocardial movement along the radial filter rays (Section II-D). Four different algorithms are implemented and tested for the regional contraction timing analysis and the derivation of a synchronicity indicator.

A. MRI Cine Acquisition and Regularization

The MRI cines for the synchronicity analysis were acquired at high temporal resolution (one hundredth of the cardiac period) on a 1.5-T MRI scanner (Gyroscan Intera, Philips Medical Systems, Best, The Netherlands) equipped with a five-element phased array coil. The pulse sequence was a segmented balanced steady-state free precession (SSFP) with a 70° flip angle and the shortest TR and TE (3.6 and 1.8 ms, respectively). For parallel imaging, sensitivity encoding (SENSE) reconstruction algorithm was used [43]. Breath hold was used to avoid motion artifacts. The MRI pulse sequence was synchronized with the cardiac cycle by vectorcardiographic (VCG) triggering. The MRI cine covered one complete cardiac cycle. Slices of 8 mm were acquired with an image resolution of 2.2 mm. The generated output images were reconstructed on a 256×256 matrix.

The LV was recorded in seven to twelve slices by scanning from base to apex along the LV long axis. According to TDI findings, a basal slice is suitable for the synchronicity analysis [15], [19]. Going from base to apex, the first slice that did not show the mitral valve structures was chosen for the synchronicity analysis. The selected slice shows a bright blood pool surrounded by darker endocardial tissue and, depending on the slice level, the structures of the papillary muscles (see Fig. 1).

The MRI cines were exported in digital imaging and communications in medicine (DICOM) format and converted into tagged image file format (TIFF) before the analysis, which was implemented in LabView® (National Instruments, Austin, TX) and Matlab® (The MathWorks, Natick, MA) software.

The resulting MRI cines are affected by two main noise sources: flow artifacts and thermal noise. Both sources cause local intensity fluctuations affecting the segmentation process and, therefore, they should be regularized. A combination of grayscale morphology closing and opening operators with a square kernel of nine spatial elements (pixels) provides an efficient regularization, proven to be more efficient than standard median filtering for the following segmentation [44]. If $O(.)$ and $C(.)$ define the opening and closing operators, and g defines the pixel gray level at the center of the operator kernel, the implemented filter, also referred to as automedian filter, determines the new value of g as $\max[O(C(O(g))), \min[g, C(O(C(g)))]]$. The combination of these complementary nonlinear filters prevents the boundary blurring observed with standard linear low-pass filters for noise suppression.

B. Definition of the Region of Interest

The tissue structures inside the LV cavity, such as the papillary muscles and the chordae tendineae, as well as the turbulent blood flow, produce intensity fluctuations in the images that may complicate the endocardial segmentation. A more robust segmentation can be obtained if a small ROI is determined that contains the endocardial boundary. This ROI can be made of two closed curves that contain the range of motion of the endocardium during the entire cardiac cycle (see Fig. 1). Here, we propose a fully automatic approach for the ROI determination.

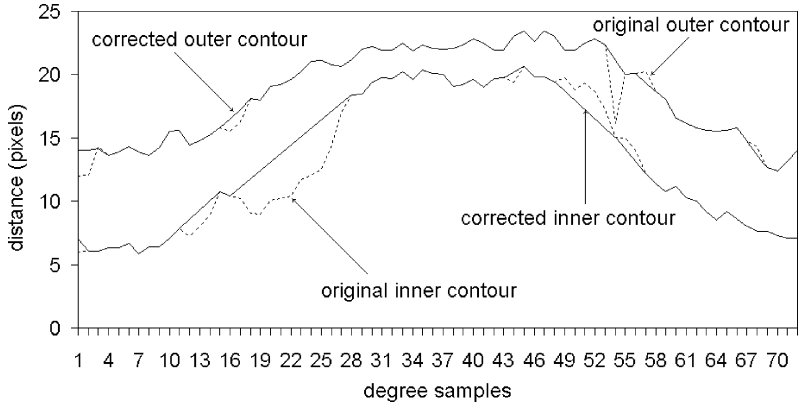

Fig. 3. Inner and outer contours for the ROI definition before and after outlier correction.

If a single frame of the cine is considered, an automatic definition of the ROI that determines the LV endocardium is complicated by the number of structures in the image that present similar features. The use of temporal information (dynamic features), instead, may provide sufficient information for the ROI definition. In particular, the myocardium (and, therefore, the endocardium) distinguishes itself from the other structures in the thorax because of its motion, which results in time-varying gray levels near the boundary between the blood pool and the endocardium. We define $I(x,y,t)$ as the time-dependent intensity signal at the spatial (pixel) coordinates (x,y).

In the literature, several algorithms are presented that derive parametric images from a model interpolation of gray-level variations [45]. However, our aim is the determination of the movement locations for the LV ROI definition, which is a preprocessing step to automate the initialization of the synchronicity analysis. In fact, the motion in the cine can also be estimated without a parametrization of $I(x,y,t)$. It can be based on the enhancement of the locations with large gray-level variations (motion energy). To this end, we estimate the variance $\sigma^2(x,y)$ of $I(x,y,t)$ as

$$\sigma^2(x,y) = \frac{1}{T}\sum_{t\in T}\left[I(x,y,t) - \overline{I}(x,y)\right]^2 \qquad (1)$$

where T and $\overline{I}$ are the signal duration (cardiac period) and average intensity, respectively.

The values of $\sigma^2(x,y)$ can be used to construct an image whose histogram is analyzed to calculate a threshold for the separation between moving and nonmoving structures. A binary image, referred to as *motion image*, is therefore generated by applying the threshold proposed by Otsu [46] [see Fig. 1(a)].

The resulting motion image is characterized by a circular shape in the foreground, which is due to the approximately concentric movement of the myocardium. However, the foreground in the motion image can be fragmented, making the recognition of the complete endocardial ROI difficult. This recognition must be, therefore, performed by a dedicated image analysis. The Hough transform (HT) is a suitable tool for detecting curves in an image [47], and it was already proposed for the recognition of endocardial structures [39], [48]. Basically, the HT is a method that tests the foreground pixels against the equation describing the investigated curve. The equation of a circle is given as $(x-x_0)^2 + (y-y_0)^2 = r^2$. In this case, the HT assigns a value (vote) to every vector (x_0, y_0, r). This vote depends on the number of foreground pixels that are intersected by the circle described by the vector (x_0, y_0, r).

In general, the center (x_0, y_0) of the circle with the highest vote corresponds to the center of the concentric motion (seed point) and its radius r corresponds to the average distance between the endocardium and the center of motion. Many different implementations exist that solve (x_0, y_0) and r. We have chosen to employ the 21-HT, since it is an efficient implementation [49]. A drawback of the 21-HT is a bias for large circles, as the result depends on the circumference [49]. However, a simple normalization of the results using the circle radius can overcome this problem [50].

The seed point with the largest vote is used to proceed with the ROI definition based on the *a priori* knowledge about the structures that are present in the image. The endocardial contour (and its motion) in a short-axis view has a smooth convex shape. This characteristic of continuity can be used as a condition to improve the ROI definition. The inner and outer points of the foreground structure are determined along a beam of rays originating from (x_0, y_0) and spanning the entire circle with a resolution of 5°. The two curves defining the ROI can be described in polar coordinates as shown in Fig. 3. They are, respectively, referred to as $r_i(\theta)$ and $r_o(\theta)$. The continuity condition corresponds to a smooth polar derivative of both $r_i(\theta)$ and $r_o(\theta)$.

Although the seed point is always inside the detected boundary curves, the magnitude of the polar derivative $dr/d\theta$ varies from zero if the seed point is not positioned in the center of the circular boundaries. Given a circle of radius r_m, the largest absolute value of the polar derivative $|dr/d\theta|_{\max}$ is obtained when the seed point is displaced by a distance r_m from the original center (worst condition), i.e., it overlaps the circumference. In this case, it can be easily proven that $|dr/d\theta|_{\max} = r_m$. For a discrete radial sampling of resolution $\Delta\theta$, the resulting polar derivative boundaries are given as

$$\left|\frac{\Delta r(\theta)}{\Delta\theta}\right| \le \left|\frac{\Delta r}{\Delta\theta}\right|_{\max} = \frac{2r_m \sin(\frac{\Delta\theta}{2})}{\Delta\theta}. \qquad (2)$$

For $\Delta\theta$ equal to 5°, $|\Delta r/\Delta\theta|_{\max} = 0.017 \cdot r_m$ pixel/°. In practice, r_m is estimated as $M^{-1} \cdot \sum_{j=1}^{M} r_j$, where M is the number of estimated radii r_j along the endocardium. For a correct ROI

definition, the edge points overtaking this threshold (outliers) are, therefore, removed. This operation allows discontinuous structures, such as the papillary muscles, to be excluded from the following endocardial segmentation. The angle to initialize the iterative outlier removal process is determined in the polar plot as the middle of the segment (corresponding to 30°) that shows the minimum variance. The outlier removal process is performed clockwise and counterclockwise until no outliers are detected.

The curves $r_i(\theta)$ and $r_o(\theta)$ are reconstructed by linear interpolation of the remaining points as shown in Fig. 3. The linear interpolation in the polar domain corresponds to a circular interpolation in the Cartesian domain, resulting in a better approximation of the smooth convex shape of the endocardial movement. The ROI $r(\theta)$ for the following segmentation is then defined as the radial area denoted by

$$r_i(\theta) \leq r(\theta) \leq r_o(\theta). \tag{3}$$

Before interpolation, the ROI is slightly expanded to ensure that the complete endocardium is included during the entire cardiac cycle. The ROI expansion is performed by a 20% contraction of $r_i(\theta)$ and a 20% expansion of $r_o(\theta)$.

Eventually, the seed point position is recalculated as the centroid of the internal ROI curve $r_i(\theta)$. This new seed point is the reference for the rest of the analysis.

C. Endocardium Detection and Tracking

The endocardium is tracked within the defined ROI for the entire cine. In general, the endocardial boundary is characterized by a sharp gray-level drop at the transition between the blood pool and the myocardium. These transitions produce high frequencies in the frequency spectrum, which can be enhanced by a monodimensional high-pass filter along the rays originating from the seed point [36]. However, the edge detection in [36] needs the definition of a threshold, which remains a critical issue due to its dependency on the image characteristics. Therefore, we propose the replacement of the radial filter in [36] by a more elaborated algorithm, which does not require the definition of a threshold.

In general, an edge detection high-pass filter must be optimized on the basis of the image characteristics, resulting in a compromise between localization accuracy and noise sensitivity. A flexible compromise, where accurate localization and noise robustness are combined, can be found using multiscale analysis. An example is given by the edge detector introduced by Canny [51], where the signal is filtered by a Gaussian filter before performing the edge estimation by image gradient analysis.

The standard deviation of the adopted Gaussian filter defines the different scales. This corresponds to the use of a Gaussian-derivative mother wavelet with unitary variance for the wavelet transform of the signal [52]. Variations of the scale parameter s, i.e., the standard deviation, provides control over the balance between noise sensitivity and localization accuracy [53]. Before being used as mother wavelet, the Gaussian derivative is adjusted, i.e., multiplied by $s^{3/2}$, in order to ensure equal energy (integral between $-\infty$ and $+\infty$ of the squared function) at

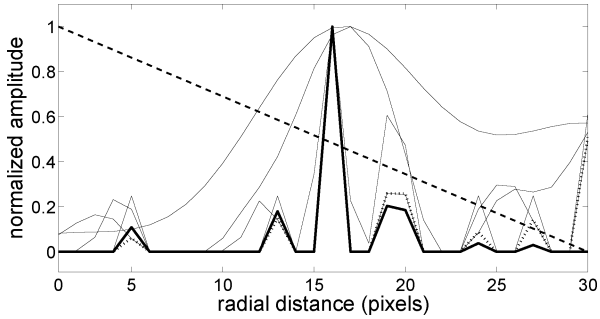

Fig. 4. Multiscale analysis of a step function $u_1(n-16)$ plus Gaussian noise (SNR = 10 dB). Five light gray curves represent the different scales. The function $\mu(n)$ is determined before (dotted black) and after (solid black) weighting by $h(n)$ (dashed black).

different scales [54]. For each scale $s \in S$, the wavelet transform yields as output

$$W(n,s) = \sum_{j=0}^{N-1} g(j) \frac{-(j-n)}{s\sqrt{2\pi}s} e^{-(1/2)((j-n)/s)^2} \tag{4}$$

where n and $j, \in [0, N-1]$, are the indices of the pixel location along a ray (radial distance), N is the number of pixels along a ray, and g defines the gray level. Negative values of $W(n,s)$ are replaced by zero. For a discrete signal of length N, the adopted number of scales is $S = \lfloor \log_2(N) + 1 \rfloor$.

Once a multiscale analysis is performed, the edges (with negative slope) for each scale correspond to the (local) maxima of $W(n,s)$ along the ray. Without the need for a threshold, the location $\widehat{n}$ along a ray of the dominant edge, i.e., the endocardium, can be defined as

$$\widehat{n} = (n : \mu(n) > \mu(m), \forall n \neq m) \tag{5}$$

where $\mu(n)$ is defined as the minimal value for all the scales of the normalized $W(n,s)$, i.e.,

$$\mu(n) = \min_S \left[W(n,s) \left(\max_N [W(n,s)] \right)^{-1} \right]. \tag{6}$$

The solution in (5) results in an efficient combination of localization accuracy, provided by the lower scales, and noise robustness, provided by the higher scales [53].

The robustness of the segmentation algorithm is further improved by exploiting spatial and temporal information. Spatial *a priori* information related to the structures that are present in the images is integrated in the system. In particular, fat tissue surrounding the myocardium results in image edges that are similar in structure to the endocardial contour. In order to avoid the detection of false edges, a linear weighting function $h(n) = 1 - n \cdot N^{-1}$ is multiplied by $\mu(n)$ before the calculation of the maximum, which is performed on $\mu'(n) = \mu(n) \cdot h(n)$. Temporal information relates to the analysis of subsequent frames. A temporal continuity assumption is integrated in the system by calculating $\mu'(n)$ over the output scales of three subsequent frames together. Temporal continuity results from the use of high temporal resolution MRI scans. Fig. 4 shows an example of multiscale analysis.

Temporal and spatial continuity are again employed to contain possible edge outliers. Low-pass zero-phase finite-impulse response (FIR) filtering is applied in time and space domain to

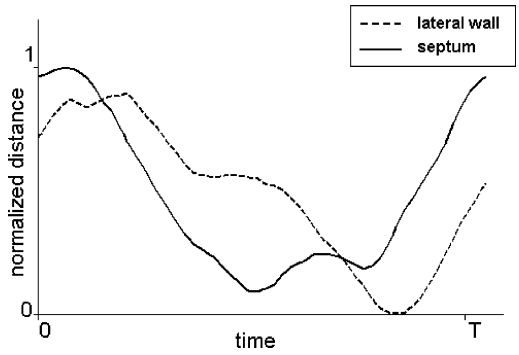

Fig. 5. Example of two dyssynchronous time-displacement curves from the lateral wall (dashed line) and the septum (solid line), respectively. T is the cardiac period.

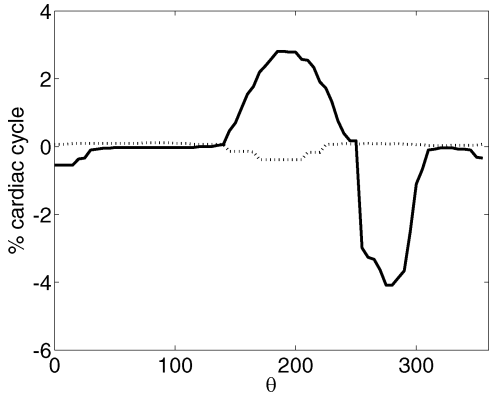

Fig. 6. Regional contraction timings for a subject with (solid) and without (dashed) LBBB. The angle θ determines the radial direction of motion.

smooth the edge variations. The cutoff frequency of the filters is equal to the fundamental frequency (heart rate) and 7.5% of the sampling frequency, respectively. Filters of a length of 15 samples were used, which appeared to be sufficient for the realization of the defined specifications. The time domain relates to the temporal sequence of frames in the MRI cine while the space domain relates to the edge detections along adjacent rays in a single frame.

D. Regional Intraventricular Dyssynchrony

The result of the segmentation algorithm is a function $r(\theta, k)$, which defines the edge distance from the seed point along a θ degree ray at the frame k. Synchronicity estimations result from the analysis of the TDCs $r(\theta, k)$ for different rays. When the seed point is not completely centered in the middle of the cavity, the TDCs are projections of the motion along the ray, which are still suitable for timing analysis. However, the spatial sampling along the endocardium would not be equally distributed and the sample location would not be fixed during the cardiac cycle. This is the main reason to adjust the seed point coordinates as described at the end of Section II-B.

To improve the accuracy of the analysis, the TDC time resolution is doubled by linear upsampling (interpolation). The TDC, as shown in Fig. 5, includes both systole (contraction) and diastole (expansion) and resembles one period of a sinusoidal function. When no conduction system dysfunction is present, the ventricle contracts synchronously along its basal segments. As a result, $r(\theta, k)$ shows a similar behavior in time for each angle. When a conduction system block is present, the TDCs for different rays may show long delays.

Some segmentation-based methods for synchronicity evaluation proposed in the literature are based on estimation of the systolic time [25]. This approach might be more susceptible to noise as it focuses only on a specific moment of the cardiac cycle (end systole). The analysis of the complete cardiac cycle has also been proposed to estimate the intraventricular dyssynchrony [39] as well as to compare lateral to septal contraction timing [26], [28]. Under the assumption of a sinusoidal TDC, the mutual phase difference was defined as the arccosine of the internal product between the lateral and septal TDCs [28]. Another approach used the internal product with a reference sine and cosine curve (one cycle) to derive an absolute phase delay [26]. These methods are, however, based on the assumption of a sinusoidal TDC and they are, therefore, sensitive to shape variations of the TDC at different angles. Shape variations are expected due to contraction differences along the myocardium, which at different locations do not follow the same dynamics.

For a complete validation of the proposed methods, both the systolic time and the inner product approaches are adapted and integrated in our MRI-cine short-axis-view analysis. The systolic time is defined as the time to the minimum value of the TDC, i.e., the end-systolic time, while the implemented inner product $\langle r(\theta_i, k), r(\theta_j, k)\rangle$ between two TDCs corresponding to the angles θ_i and θ_j is implemented as

$$\langle r(\theta_i,k), r(\theta_j,k)\rangle = \frac{\sum_{k=0}^{N-1} r(\theta_i,k)\cdot r(\theta_j,k)}{\sqrt{\sum_{k=0}^{N-1} r(\theta_i,k)^2 \cdot \sum_{k=0}^{N-1} r(\theta_j,k)^2}}. \quad (7)$$

In this paper we present an alternative approach based on the cross correlation of all the TDCs with a reference TDC derived from the measured curves. For an accurate measurement, the reference curve should show large amplitude and signal-to-noise ratio (SNR). The output of a temporal low-pass filter applied to $r(\theta, k)$ is considered as the noise-free signal. Therefore, the SNR is defined as the ratio between the variance of the output and of the difference between input and output of this filter. The TDC amplitude is defined as the variance of the filter output. Eventually, the reference TDC is determined as the curve displaying the best amplitude and SNR characteristics. The same reference TDC is also used for the application of the inner product method in (7).

Once a reference is determined, the regional contraction timing is defined as the time at which the cross correlation with the reference curve shows its maximum. The regional contraction timing is defined for each ray. Typically, 72 rays are employed to span the entire circle. Fig. 6 shows a regional contraction timing plot for two subjects with and without an LBBB. The contraction timing in the presence of an LBBB shows increased variations.

CHF patients often present a dilated LV, where the septum thickness and function is significantly reduced. As a result, the septal movement becomes sensitive to the pressure gradient between right and left ventricles [40]. This passive pressure-driven

septal movement is known as paradoxical movement. The septal TDC $r(\theta_0, k)$ can be approximated as

$$r(\theta_0, k) = A_a \cos(2\pi f k) + A_p \cos(2\pi f k + \phi) \qquad (8)$$

where A_a and A_p are the amplitude of the active and paradoxical movements, respectively, f is the cardiac frequency (heart rate), ϕ is the phase difference between active and paradoxical movements, and k is the discrete time. Unfortunately, the phase difference between the two movements is often close to π, making the separation of the two components impossible.

In order to avoid erroneous timing estimations due to paradoxical movements, a confidence time window is applied on the cross-correlation result before the determination of the maximum. Maxima outside the window are rejected. The window is dynamically centered on the time corresponding to the cross-correlation maximum estimated on the adjacent ray and covers one quarter of the cardiac period. This ensures cross-correlation maxima due to abrupt timing discontinuities between contiguous rays, e.g., due to contra-phase paradoxical movements, do not affect the timing measurement. The initialization is performed on the lateral wall segment, where no paradoxical movement is present.

The implemented cross-correlation method has an implicit limitation: the accuracy of the contraction timing estimates is limited by the sampling period of the signals. This problem can be overcome by phase spectrum analysis. If a discrete Fourier transform of two TDCs $r(\theta_i, k)$ and $r(\theta_j, k)$ is performed, the difference of the phase spectra results in an approximate straight line. This is because $r(\theta_i, k)$ and $r(\theta_j, k)$ are time translations of the same curve. If the slope $\Delta\phi$ of the phase difference line is determined, then the delay between $r(\theta_i, k)$ and $r(\theta_j, k)$ can be estimated with no time resolution constraints as $\Delta\phi \cdot \Delta t$, where Δt is the sampling period.

The phase analysis is performed after the cross-correlation realignment. As a result, the phase difference is bounded between $-\pi$ and π without involving wraparound of the phase within this interval due to larger delays. As already discussed, the assumption of a pure temporal translation is not completely fulfilled, and the phase difference line may show a poor SNR. A least square error method is, therefore, a suitable solution for the interpolation of the phase difference line, whose slope $\Delta\phi$ can be estimated by a weighted linear regression [42]. The weights for the linear regression are derived by the analysis of the amplitude of the frequency spectrum. They are determined as the minimum value between the amplitudes of the spectra of the two time-displacement curves. As a result, the higher energy components, which typically represent the displacement signal, contribute more to the estimation of the regression line.

Fig. 7 shows the result of a linear regression to a simulated phase difference data set with and without weighting function. One period of a 1-Hz cosine was generated with a sampling frequency of 80 Hz and shifted half sampling period after addition of white noise (SNR = 60 dB). Before applying the linear regression to the phase spectra difference between the two cosines (plus noise), the same type of noise was again added to the shifted cosine. The weighted linear regression approximates the real delay of 6.25 ms with an error of 0.23 ms against 1.5 ms for the nonweighted linear regression. According to our simulations, a similar improvement is consistent for different noise sequences.

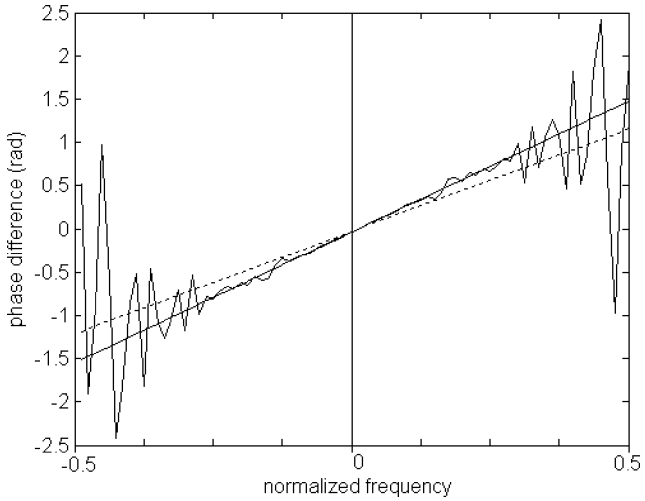

Fig. 7. Simulation of a linear regression to the phase difference of two cosines (plus noise) of one period with (solid line) and without (dashed line) weighting function. One cosine is delayed half sampling period. A better fit for the low frequencies representing the cosine function is obtained by the weighted linear regression.

III. Results

Eighteen subjects (11 with and seven without an LBBB) were tested for quantification of the regional contraction timings in an MRI short-axis basal view. All the MRI scans were performed at the Catharina Hospital, Eindhoven, The Netherlands. LBBB was diagnosed by analysis of the echocardiographic QRS duration. In three MRI cines (16.7%), the definition of the ROI failed due to an incorrect motion estimation. These three subjects (two with LBBB) were excluded from further analysis.

The performance of the proposed segmentation method was validated on four image frames per cardiac cycle. These images were selected at each quarter of the cardiac cycle starting with the first frame of the cine (end diastole). A total number of 60 images were evaluated by measuring the absolute area difference between manually and automatically delineated endocardial boundaries. The area was defined as the surface that was delimited by the delineated boundary and the area difference (absolute area error) was defined as the area that was covered by only one of the two delineations. The manual segmentation was taken as the reference method because no gold standard for segmentation of cardiac images exists. The results are shown in Fig. 8, also including a Bland–Altman analysis of the absolute area error as a percentage of the average area estimates (average between the manual and the automatic estimates) [55]. The average absolute area error is 9.82% while the corresponding standard deviation remains less than 3.76%. The correlation coefficient between the automatic and manual area estimates is 0.99, and the regression line has an angular coefficient and a bias equal to 1.009 and 1.3, respectively. These values confirm the accuracy of the presented segmentation, which is, therefore, suitable for cardiac function studies and, in particular, for cardiac synchronicity analysis [36].

The validation of the dyssynchrony analysis was performed by estimating the standard deviation of the regional contraction timing assessed by the systolic time, inner product, cross correlation, and phase difference method. These standard deviations (indicators) were derived for each subject in order to evaluate

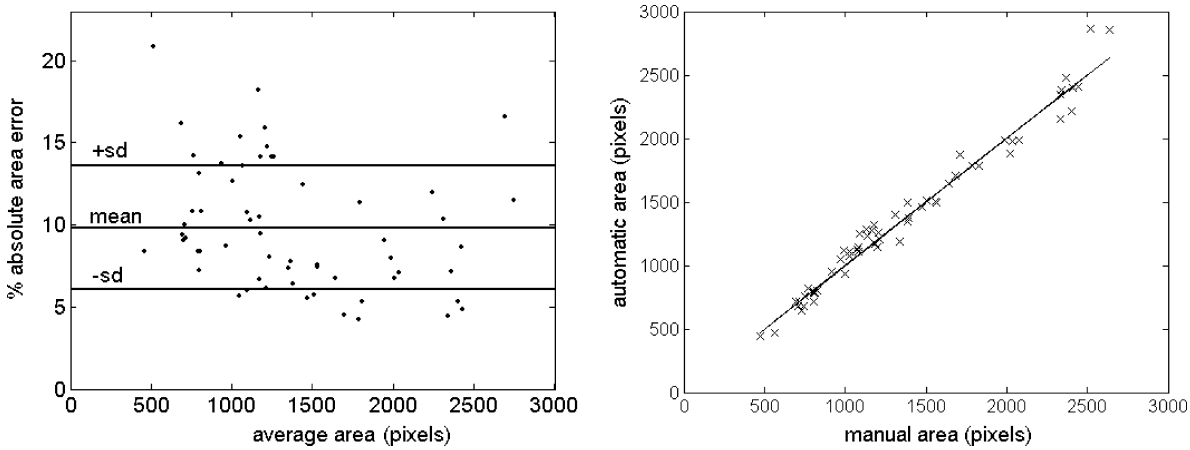

Fig. 8. (a) Bland–Altman plot of the absolute area error between automatic and manual contour segmentation. (b) Automatically estimated areas are plotted against the manually determined ones. The solid line represents the ideal equality between the estimates. This line almost coincides with the regression line, whose angular coefficient and bias equal 1.009 and 1.3, respectively.

TABLE I
MEAN AND STANDARD DEVIATION OF THE FOUR INDICATORS

Method	LBBB	Normals
Systolic time	0.1632 ± 0.0592	0.0317 ± 0.0108
Inner product	0.1021 ± 0.0385	0.0417 ± 0.0251
Cross correlation	0.1176 ± 0.0455	0.0247 ± 0.0197
Phase difference	0.1287 ± 0.0289	0.0265 ± 0.0135

their diagnostic value for LBBB patients. In Table I, the population averages and standard deviations for the four indicators are given. All the values are reported as a fraction of the cardiac cycle. The values indicate that all the indicators show separable ranges for either population (with and without LBBB).

The evaluation of a diagnostic method is typically based on sensitivity and specificity analysis. To this end, a threshold must be defined that is used to decide whether a patient has an LBBB. Despite the small statistical samples, we assume them to be represented by Gaussian distributions defined by the means and standard deviations in Table I. Inference by Bayes rule can be used to obtain the posterior class probability (normals and LBBB) by each of the four methods [56]. If C_1 and C_2 represent, respectively, the class of normals and LBBB patients, the posterior class probability P is defined as $P(C_i|x)$, where x is the dyssynchrony indicator (i.e., the measured standard deviation) and $i \in [1,2]$. Fig. 9 shows the posterior class probability $P(C_2|x)$ for the phase difference method.

The discrimination boundary between the two classes is defined as the threshold x_t such that $P(C_1|x_t) = P(C_2|x_t) = 0.5$. The thresholds for the systolic time, inner product, cross correlation, and phase difference method are 0.0592, 0.0720, 0.0602, and 0.0618, respectively. Still under the assumption of a Gaussian distribution for the two classes, specificity and sensitivity are given as the integralsof $P(C_1|x)$ between $-\infty$ and x_t and of $P(C_2|x)$ between x_t and ∞, respectively. The results for the four methods are summarized in Table II. In addition, in order to provide a graphical summary of the results, the derived specificity and sensitivity are represented in the receiver operating characteristic (ROC) space in Fig. 10 together with the ROC curves for all the four methods [57]. Although all the methods present satisfactory results, the phase method results

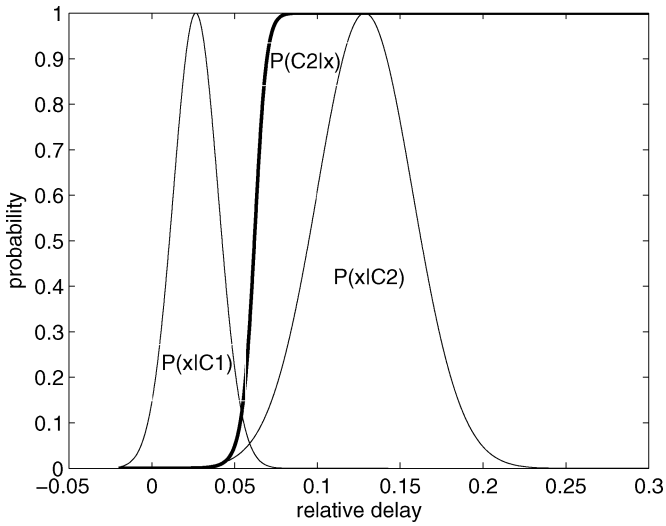

Fig. 9. Probability distribution of the classes of normals $[P(x|C_1)]$ and LBBB $[P(x|C_2)]$ subjects (amplitude normalized to one) together with the posterior probability $P(C_2|x)$.

TABLE II
SPECIFICITY AND SENSITIVITY OF THE FOUR INDICATORS

Method	Specificity	Sensitivity
Systolic time	99.5 %	96.1 %
Inner product	87.2 %	78.7 %
Cross correlation	96.5 %	89.6 %
Phase difference	99.7 %	99.0 %

in a better specificity and sensitivity. This can be easily recognized in the ROC space, where the curve related to the phase difference method shows the largest distance from the line of no discrimination (dashed line in Fig. 10).

IV. DISCUSSION AND CONCLUSION

A novel method is presented that permits the automatic evaluation of the intraventricular mechanical synchronicity based on a high time-resolution MRI cine of a short-axis basal view. The image segmentation is fully automatic and does not require user interaction for the input of landmarks. The endocardial contour

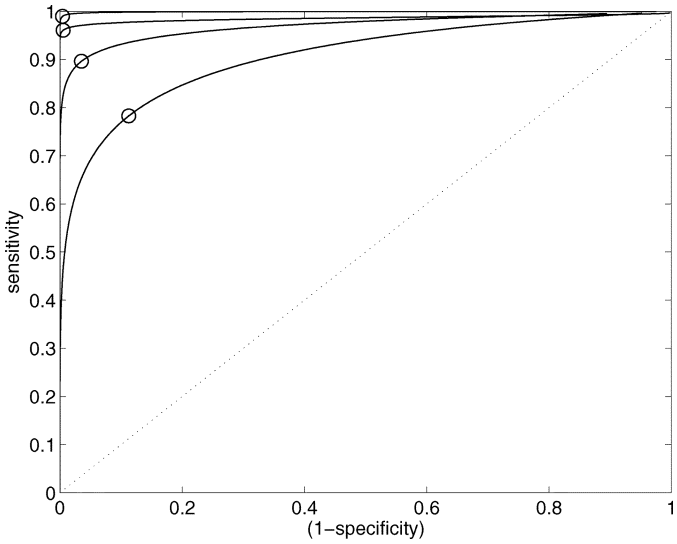

Fig. 10. Representation of the specificity and sensitivity of the methods in the ROC space. From lower to higher, the four ROC curves (solid lines) correspond to the inner product, cross correlation, systolic time, and phase difference method, respectively. The circles represent the points on the ROC curves corresponding to the optimal thresholds. The dashed line represents the line of no discrimination.

is detected without the need for a threshold by means of multiscale analysis. The evaluation of the segmentation algorithm confirmed its usability for contraction timing analysis.

After segmentation, TDCs are defined along 72 rays equally distributed along the endocardial contour. The analysis of these curves permits the definition of indicators that may have prognostic value for decision making during CRT. Four algorithms have been implemented for the curve analysis. They are based, respectively, on systolic time, inner product, cross correlation, and phase difference analysis. Validation on 15 patients showed that all methods are suitable for LBBB detection based on the standard deviation of the estimated regional contraction timings. The analysis of the entire cardiac cycle by phase difference analysis seems, however, to be the most promising in terms of sensitivity and specificity.

The improved results obtained by the phase difference against the inner product and cross-correlation methods were expected. Improved performance can be attributed to the incorrect assumption of a sinusoidal TDC on which the inner product method is based and the limited time resolution of the cross-correlation method. Compared to other dyssynchrony indicators based on a single moment of the cardiac cycle, the analysis of the complete cardiac cycle represents a valid alternative, which might also show interesting predictive value for the selection of CRT responders.

Once all the TDCs are available for all basal segments with a high spatial resolution, local indicators to guide the CTR could be defined. When a local analysis is required, the definition of a reference ray that determines a specific anatomical reference becomes important. As a result, each ray would determine a specific part of a basal segment. Although the orientation of the ventricle in the image can be standardized during MRI acquisition, the implementation of an automatic routine for an image orientation control would be desirable. The orientation analysis could be combined with the determination of the right ventricle, possibly resulting in new opportunities for interventricular synchronicity analysis based on the extension of the same algorithm.

It is known that the ventricle orientation also varies during the cardiac cycle, as the ventricular movement comprises a twist about its long axis. This twist is, however, limited to less than 5° in the basal plane (it increases to more than 10° towards the apex) [58], and it is, therefore, negligible for the presented basal synchronicity analysis. Another effect that might, however, affect the measurement is the longitudinal motion of the ventricle [59]. The effect on the synchronicity analysis of long-axis shortening and lengthening should be investigated in future study. To this end, the analysis should be also extended to the adjacent MRI short-axis slices. Ventricular translations are negligible due to the breath-hold MRI acquisition.

In general, the presented validation in patients confirms the feasibility and potential of the method, but it does not provide sufficient data to provide clinical indications. The comparison with other methods must be certainly extended to a larger population. The extension of the validation could also include other imaging techniques, such as computed tomography. Echography could be also considered; however, despite a high temporal resolution, accurate image segmentation and timing assessment could be more difficult to achieve due to the low SNR of echographic images and to motion artifacts, respectively.

Although a more extensive validation is needed, the obtained results suggest that the cardiac synchronicity can be simply evaluated by image segmentation on a short-axis view. The proposed mechanical synchronicity analysis might, therefore, provide a simple solution to some of the limitations of electrocardiogram (ECG)-based indicators.

REFERENCES

[1] T. Thom, N. Haase, W. Rosamond, V. J. Howard, J. Rumsfeld, T. Manolio, Z.-J. Zheng, K. Flegal, C. O'Donnell, S. Kittner, D. Lloyd-Jones, D. C. Goff, Jr., Y.-H. R. Adams, G. Friday, K. Furie, P. Gorelick, B. Kissela, J. Marler, J. Meigs, V. Roger, S. Sidney, P. Sorlie, J. Steinberger, S. Wasserthiel-Smoller, M. Wilson, and P. Wolf, "Heart disease and stroke statistics, 2006 update," *Circulation*, vol. 113, pp. 85–151, Jan. 2006.

[2] S. Iuliano, S. G. Fisher, P. E. Karasik, R. D. Flethter, and S. N. Singh, "QRS duration and mortality in patients with congestive heart failure," *Amer. Heart J.*, vol. 143, pp. 1085–1091, Jan. 2002.

[3] G. Bleeker, M. Schalij, S. Molhoek, H. Verwey, E. Holman, E. Boersma, P. Steendijk, E. V. D. Wall, and J. Bax, "Relationship between QRS duration and left ventricular dyssynchrony in patients with end-stage heart failure," *J. Cardiovasc. Electrophysiol.*, vol. 15, no. 5, pp. 544–549, May 2004.

[4] A. Auricchio, C. Fantoni, F. Regoli, C. Carbucicchio, A. Goette, C. Geller, M. Kloss, and H. Klein, "Characterization of left ventricular activation in patients with heart failure and left bundle-branch block," *Circulation*, vol. 109, no. 9, pp. 1133–1139, Mar. 2004.

[5] C. Grines, T. Bashore, H. Boudoulas, S. Olson, P. Shafer, and C. Wooley, "Functional abnormalities in isolated left bundle branch block, the effect of interventricular asynchrony," *Circulation*, vol. 79, no. 4, pp. 845–853, Apr. 1989.

[6] W. Little, R. Reeves, J. Arciniegas, R. Katholi, and E. Rogers, "Mechanism of abnormal interventricular septal motion. During delayed left ventricular activation," *Circulation*, vol. 65, no. 7, pp. 1486–1491, Jun. 1982.

[7] M. S. J. Sutton, T. Plappert, W. Abraham, A. Smith, D. DeLurgio, A. Leon, E. Loh, D. Kocovic, W. Fisher, M. Ellestad, J. Messenger, K. Kruger, K. Hilpisch, and M. Hill, "Effect of cardiac resynchronization therapy on left ventricular size and function in chronic heart failure," *Circulation*, vol. 107, no. 15, pp. 1985–1990, 2003.

[8] M. S. J. Sutton and M. Keane, "Reverse remodeling in heart failure with cardiac resynchronization therapy," *Heart*, vol. 93, no. 2, pp. 167–171, Feb. 2007.

[9] W. T. Abraham, W. G. Fisher, A. L. Smith, D. B. Delurgio, A. R. Leon, E. Loh, D. Z. Kocovic, M. Packer, A. L. Clavell, D. L. Hayes, M. Ellestad, R. J. Trupp, J. Underwood, F. Pickering, C. Truex, P. McAtee, and J. Messenger, "Cardiac resinchronization in chronic heart failure," *New Eng. J. Med.*, vol. 346, no. 24, pp. 1845–1853, 2002.

[10] J. Cleland, J. Daubert, E. Erdman, N. Freemantle, D. Gras, L. Kappenberger, and L. Tavazzi, "The effect of cardiac resynchronization on morbidity and mortality in heart failure," *New Eng. J. Med.*, vol. 52, no. 15, pp. 1539–1549, 2005.

[11] C. C. Leclercq and D. Kass, "Retiming the failing heart: Principles and current clinical status of cardiac resynchronization," *J. Amer. Coll. Cardiol.*, vol. 39, no. 2, pp. 194–201, Jan. 2002.

[12] J. Bax, T. Abraham, S. Barold, O. Breithardt, J. Fung, S. Garrigue, J. G. , III, D. Hayes, D. Kass, J. Knuuti, C. Leclercq, C. Linde, D. Mark, M. Monaghan, P. Nihoyannopoulos, M. Schalij, C. Stellbrink, and C. Yu, "Cardiac resynchronization therapy: Part 1 – Issues before device implantation," *J. Amer. Coll. Cardiol.*, vol. 46, no. 12, pp. 2153–2167, Dec. 2005.

[13] A. Kashani and S. Barold, "Significance of QRS complex duration in patients with heart failure," *J. Amer. Coll. Cardiol.*, vol. 46, no. 12, pp. 2183–2192, Dec. 2005.

[14] M. V. Pitzalis, M. Iacoviello, R. Romito, F. Massari, B. Rizzon, G. Luzzi, P. Guida, A. Andriani, F. Mastropasqua, and P. Rizzon, "Cardiac resynchronization therapy tailored by echocardiographic evaluation of ventricular asynchrony," *J. Amer. Coll. Cardiol.*, vol. 40, no. 3, pp. 1615–1622, 2002.

[15] C.-M. Yu, W.-H. Fung, H. Lin, Q. Zhang, J. E. Sanderson, and C.-P. Lau, "Predictors of left ventricular reverse remodeling after cardiac resynchronization therapy for heart failure secondary to idiopathic dilated or ischemic cardiomiopathy," *Amer. J. Cradiol.*, vol. 91, pp. 684–688, 2002.

[16] P. Sogaard, H. Egeblad, W. Y. Kim, H. K. Jensen, A. K. Pederson, B. O. Kristensen, and P. T. Mortensen, "Tissue doppler imaging predicts improved systolic performance and reversed left ventricular remodeling during long-term cardiac resynchronization therapy," *J. Amer. Coll. Cradiol.*, vol. 40, no. 4, pp. 723–730, 2002.

[17] C.-M. Yu, H. Lin, and J. E. Sanderson, "High prevalence of left ventricular systolic and diastolic asynchrony in patients with congestive heart failure and normal QRS duration," *Heart*, vol. 89, pp. 54–60, 2003.

[18] W. Abraham, "Cardiac resinchronization therapy: A review of clinical trials and criteria for identifying the appropriate patient," *Rev. Cardiovasc. Med.*, vol. 4, no. 2, pp. S30–S37, 2003.

[19] A. H. M. Jansen, F. Bracke, J. M. van Dantzig, A. Meijer, H. H. M. Korsten, K. H. Peels, and N. M. van Hemel, "Optimization of pulsed wave tissue Doppler to predict left ventricular reverse remodeling after cardiac resynchronization therapy," *J. Amer. Soc. Echocardiogr.*, vol. 19, no. 2, pp. 185–191, 2006.

[20] M. Penicka, J. Bartunek, B. D. Bruyne, M. Vanderheyden, M. Goethals, M. D. Zutter, P. Brugada, and P. Geelen, "Improvement of left ventricular function after cardiac resynchronization therapy is predicted by tissue Doppler imaging echocardiography," *Circulation*, vol. 109, no. 8, pp. 978–983, 2004.

[21] C. Yu, J. Fung, Q. Zhang, C. Chan, Y. Chan, H. Lin, L. Kum, S. Kong, Y. Zhang, and J. Sanderson, "Tissue dDoppler imaging is superior to strain rate imaging and postsystolic shortening on the prediction of reverse remodeling in both ischemic and nonischemic heart failure after cardiac resynchronization therapy," *Circulation*, vol. 110, no. 1, pp. 66–73, 2004.

[22] C.-M. Yu, E. Chau, J. E. Sanderson, M.-O. T. K. Fan, W.-H. Fung, H. Lin, S.-L. Kong, Y.-M. Lam, M. R. S. Hill, and C.-P. Lau, "Tissue Doppler echocardiographic evidence of reverse remodeling and improved synchronicity by simultaneously delaying regional contraction after biventricular pacing therapy in heart failure," *Circulation*, vol. 105, pp. 438–445, 2002.

[23] A. Lardo, T. Abraham, and D. Kass, "Magnetic resonance imaging assessment of ventricular dyssynchrony: Current and emerging concepts," *J. Amer. Coll. Cardiol.*, vol. 46, no. 12, pp. 2223–2228, Dec. 2005.

[24] V. M. Pai and L. Axel, "Advances in MRI tagging techniques for determining regional myocardial strain," *Current Cardiol. Rep.*, vol. 8, no. 1, pp. 53–58, 2006.

[25] S. Kapetanakis, M. T. Kearney, A. Siva, N. Gall, M. Cooklin, and M. J. Monaghan, "Real-time three-dimensional echocardiography: A novel technique to quantify global left ventricular mechanical dyssynchrony," *Circulation*, vol. 112, no. 7, pp. 992–1000, Aug. 2005.

[26] O. A. Breithardt, C. Stellbrink, A. P. Kramer, A. M. Sinha, A. Franke, R. Salo, B. Schiffgens, E. Huvelle, and A. Auricchio, "Echocardiographic quantification of left ventricular asynchrony predicts an acute hemodynamic benefit of cardiac resynchronization therapy," *J. Amer. Coll. Cardiol.*, vol. 40, no. 3, pp. 536–545, Aug. 2002.

[27] T. Fujino, S. Ono, K. Murata, N. Tanaka, T. Tone, T. Yamamura, Y. Tomochika, K. Kimura, K. Ueda, J. Liu, Y. Wada, M. Murashita, Y. Kondo, and M. Matsuzaki, "New method of on-line quantification of regional wall motion with automated segmental motion analysis," *J. Amer. Soc. Echocardiogr.*, vol. 14, no. 9, pp. 892–901, Sep. 2001.

[28] O. Grebe, A. Müller, N. Merkle, J. Wöhrle, L. Binner, M. Höher, V. Hombach, H. Neumann, and H. Kestler, "Estimation of intra- and interventricular dyssynchronization with cardiac magnetic resonance imaging," in *Proc. Comput. Cardiol.*, Thessaloniki, Sep. 2003, vol. 30, pp. 741–743.

[29] A. Frangi, W. Niessen, and M. Viergever, "Three-dimensional modeling for functional analysis of cardiac images: A review," *IEEE Trans. Med. Imag.*, vol. 20, no. 1, pp. 2–25, Jan. 2001.

[30] A. P. Dhawan, *Medical Image Analysis* . New York: Wiley, 2003.

[31] T. F. Cootes, G. J. Gareth, and C. J. Taylor, "Active appearance models," *IEEE Trans. Patterns Anal. Mach. Intell.*, vol. 23, no. 6, pp. 681–685, Jun. 2001.

[32] B. van Ginneken, A. F. Frangi, J. J. Staal, B. M. ter Haar Romeny, and M. A. Viergever, "Active shape model segmentation with optimal features," *IEEE Trans. Med. Imag.*, vol. 21, no. 8, pp. 924–933, Aug. 2002.

[33] H. El-Messiry, H. Kestler, O. Grebe, and H. Neumann, "Segmenting the endocardial border of the left ventricle in cardiac magnetic resonance images," *Comput. Cardiol.*, vol. 30, pp. 625–628, 2003.

[34] M. Kass, A. Witkin, and D. Terzopoulos, "Snakes: Active contour models," *Int. J. Comput. Vis.*, vol. 1, no. 4, pp. 321–331, 1987.

[35] S. Osher and J. Sethiam, "Fronts propagating with curvature-dependent speed: Algorithms based on Hamilton-Jacobi formulation," *J. Comput. Phys.*, vol. 79, pp. 12–49, 1988.

[36] M. Mischi, A. A. C. M. Kalker, and H. H. M. Korsten, "Cardiac image segmentation for contrast agent videodensitometry," *IEEE Trans. Biomed. Eng.*, vol. 52, no. 2, pp. 277–286, Feb. 2005.

[37] S. K. Setarehdan and J. J. Soraghan, "Automatic cardiac LV boundary detection and tracking using hybrid fuzzy temporal and fuzzy multiscale edge detection," *IEEE Trans. Biomed. Eng.*, vol. 46, no. 11, pp. 1364–1378, Nov. 1999.

[38] M. Sezgin and B. Sankur, "Survey over image thresholding techniques and quantitative performance evaluation," *J. Electron. Imag.*, vol. 13, no. 1, pp. 146–168, Jan. 2004.

[39] A. Müller, A. Neitmann, N. Merkle, J. Wöhrle, V. Hombach, and H. Kestler, "Contour detection of short axis slice mr images for contraction irregularity assessment," *Comput. Cardiol.*, vol. 32, pp. 21–24, 2005.

[40] A. S. Abbasi, L. M. Eber, R. N. Macalpin, and A. A. Kattus, "Paradoxical motion of interventricular septum in left bundle branch block," *Circulation*, vol. 49, no. 14, pp. 423–427, 1974.

[41] H. Tanaka, C. Tei, S. Nakao, M. Tahara, S. Sakurai, T. Kashima, and T. Kanehisa, "Diastolic bulging of the interventricular septum toward the left ventricle. An echocardiographic manifestation of negative interventricular pressure gradient between left and right ventricles during diastole," *Circulation*, vol. 62, pp. 558–563, 1980.

[42] C. J. Houtman, D. F. Stegeman, J. P. van Dijk, and M. J. Zwarts, "Changes in muscle fiber conduction velocity indicate recruitment of distinct motor unit populations," *J. Appl. Physiol.*, vol. 95, pp. 1045–1054, 2003.

[43] K. Pruessmann, M. Weiger, M. Scheidegger, and P. Boesiger, "Sense: Sensivity encoding for fast MRI," *Magn. Resonan. Med.*, vol. 42, no. 5, pp. 952–962, 1999.

[44] R. M. Haralick, S. R. Sternberg, and X. Zhuang, "Image analysis using mathematical morphology," *IEEE Trans. Pattern. Anal. Mach. Intell.*, vol. PAMI-9, no. 4, pp. 532–550, Jul. 1987.

[45] C. R. Dominguez, N. Kachenoura, A. D. Cesare, A. Delouche, P. Lim, O. Gerard, A. Herment, B. Diebold, and F. Frouin, "Assessment of left ventricular contraction by parametric analysis of main motion (PAMM): Theory and application for echocardiography," *Phys. Med. Biol.*, vol. 50, no. 14, pp. 3277–3296, 2005.

[46] N. Otsu, "Threshold selection method from gray-level histograms," *IEEE Trans. Syst. Man. Cybern.*, vol. SMC-9, no. 1, pp. 62–66, Jan. 1979.

[47] R. O. Duda and P. E. Hart, "Use of the Hough transformation to detect lines and curves in pictures," *Comm. ACM*, vol. 15, pp. 11–15, 1972.

[48] A. Müller, A. Neitmann, M. Kunze, N. Merkle, M. Höher, V. Hombach, J. Wöhrle, H. Neumann, and H. Kestler, "Integrating model based and data driven approaches for the automatic segmentation of cardiac short-axis cine MRI recordings," *Comput. Cardiol.*, vol. 33, pp. 73–76, 2006.

[49] H. K. Yuen, J. Princen, J. Illingworth, and J. Kittler, "Comparative study of Hough transform methods for circle finding," *Image Vis. Comput.*, vol. 8, no. 1, pp. 71–77, Feb. 1990.

[50] D. Ioannou, W. Huda, and A. F. Laine, "Circle recognition through a 2D Hough transform and radius histogramming," *Image Vis. Comput.*, vol. 17, no. 1, pp. 15–26, Jan. 1999.

[51] J. Canny, "A computational approach to edge detection," *IEEE Trans. Pattern. Anal. Mach. Intell.*, vol. PAMI-8, no. 6, pp. 679–698, Nov. 1986.
[52] L. Bruce and J. Li, "Wavelets for computationally efficient hyperspectral derivative analysis," *IEEE Trans. Geosci. Remote Sens.*, vol. 39, no. 7, pp. 1540–1546, Jul. 2001.
[53] S. Mallat and S. Zhong, "Characterization of signals from multiscale edges," *IEEE Trans. Pattern. Anal. Mach. Intell.*, vol. 14, no. 7, pp. 710–732, Jul. 1992.
[54] L. Sörnmo and P. Laguna, *Bioelectrical Signal Processing in Cardiac and Neurological Applications*. New York: Academic, 2005.
[55] J. Bland and D. Altman, "Statistical methods for assessing agreement between two methods of clinical measurement," *Lancet*, vol. 327, no. 8476, pp. 307–310, Feb. 1986.
[56] R. O. Duda, P. E. Hart, and D. G. Stork, *Pattern Classification*, 2nd ed. New York: Wiley, 2001.
[57] H. Zweig and G. Campbell, "Receiver-operating characteristic (ROC) plots: A fundamental evaluation tool in clinical medicine," *Clin. Chem.*, vol. 39, pp. 561–577, 1993.
[58] A. S. Abbasi, L. M. Eber, R. N. Macalpin, and A. A. Kattus, "New noninvasive method for assessment of left ventricular rotation," *Circulation*, vol. 112, pp. 3149–3156, 2005.
[59] P. P. Sengupta, B. K. Khandheria, J. Korinek, J. Wang, A. Jahangir, J. B. Seward, and M. Belohlavek, "Apex-to-base dispersion in regional timing of left ventricular shortening and lengthening," *J. Amer. Coll. Cardiol.*, vol. 47, no. 1, pp. 163–172, 2006.

Massimo Mischi (M'04) was born in Rome, Italy, in 1973. He received the M.Sc. degree in electrical engineering from La Sapienza University, Rome, Italy, in 1999. He completed a two-year Post-Master program in technological design, information and communication technology, in 2002 and received the Ph.D. degree in 2004 from the Eindhoven University of Technology, Eindhoven, The Netherlands. His work concerned the development of cardiovascular diagnostic methods by means of contrast ultrasonography.

In 2000, he became a Research Assistant at the Eindhoven University of Technology, where he is currently an Assistant Professor. His research covers several topics in the field of biomedical signal processing.

Harrie C. M. van den Bosch was born in Eindhoven, The Netherlands, in 1965. He studied medicine at the University of Nijmegen, The Netherlands, and was trained as a Radiologist at the Catharina Hospital, Eindhoven, The Netherlands. He completed a one-year fellowship in cardiovascular MR at the University of Leiden, The Netherlands.

Since 1999, he has been a Radiologist at the Catharina Hospital and Director of Cardiovascular MR, Eindhoven, The Netherlands. He is an active member of the Society for Cardiovascular Magnetic Resonance (SCMR), the North American Society for Cardiac Imaging (NASCI), the Workgroup CMR of the European Society of Cardiology (ESCR), the Cardiac study group of the International Society for Magnetic Resonance in Medicine (ISMRM), founding member of the European Chapter of the SCMR, and boardmember of the Cardiovascular section of the Dutch radiology Society.

Annemieke H. M. Jansen was born in The Netherlands in 1965. She studied medicine at the University of Maastricht, The Netherlands. She was trained as a Cardiologist at the Catharina Hospital, Eindhoven The Netherlands, where she is currently working towards the Ph.D. degree in echocardiography for predicting the response to cardiac resynchronization therapy.

Mischa Sieben was born in Eindhoven, The Netherlands, in 1976. He received the B.S. degree in electric and electronic engineering from the Fontys Hogescholen Eindhoven, Eindhoven, The Netherlands, in 2000 and the M.S. degree in electrical engineering from the Eindhoven University of Technology, Eindhoven, The Netherlands, in 2005, where he is currently working towards the Ph.D. degree in technology design, information and communication technology.

Until July 2006, he was a Research Assistant at the Eindhoven University of Technology, working on the assessment of regional wall motion of the left ventricle in order to study the synchronicity of the contraction.

Ronald M. Aarts (M'95–SM'95–F'07) was born in Amsterdam, The Netherlands, in 1956. He received the B.Sc. degree in electrical engineering and the Ph.D. degree in physics from the Delft University, Delft, The Netherlands, in 1977 and 1995, respectively.

He joined Philips Research Laboratories in 1977, working on various DSP-algorithms and applications. He is a part-time Full Professor at the Eindhoven University of Technology, Eindhoven, The Netherlands. In 2003, he extended his interests in engineering to medicine. He has published a large number of papers and reports and holds over one hundred granted and pending U.S. patents in these fields.

Dr. Aarts is a Fellow of Audio Engineering Society (AES).

Hendrikus H. M. Korsten was born in The Netherlands in 1953. He studied medicine at the University of Groningen, The Netherlands, and graduated as a Medical Doctor in 1978. During his training as an Anesthesiologist at the University of Utrecht, The Netherlands, he started the Ph.D. study on the measurement of intrathoracic fluid content during open-heart surgery. He received the Ph.D. degree in medicine form the University of Leiden, Leiden, The Netherlands, in 1984.

Since June 1982, he has been a Staff Member at the Department of Anesthesiology, Intensive Care and Pain-Treatments, Catharina Hospital, Eindhoven, The Netherlands. From 1989 until 1993, he was the Chairman of the professional medical staff of this hospital. He is also an Intensivist and was Head of the Intensive Care during 1993–2001. He was one of the initiators of a national intensive-care database. He was also involved in research projects on data storage and data mining of patient data, as well as the development of artificial intelligence in the intensive care. In 2001, he was appointed Professor at the Department of Electrical Engineering, Eindhoven University of Technology, Eindhoven, The Netherlands.